

# A Very High Energy Gamma-Ray Spectrum of 1ES 2344+514

M. Schroedter<sup>1,2</sup>, H. M. Badran<sup>3</sup>, J. H. Buckley<sup>4</sup>, J. Bussons Gordo<sup>5</sup>, D. A. Carter-Lewis<sup>2</sup>, C. Duke<sup>6</sup>, D. J. Fegan<sup>7</sup>, S. F. Fegan<sup>8</sup>, J. P. Finley<sup>9</sup>, G. H. Gillanders<sup>10</sup>, J. Grube<sup>11</sup>, D. Horan<sup>1</sup>, G. E. Kenny<sup>10</sup>, M. Kertzman<sup>12</sup>, K. Kosack<sup>4</sup>, F. Krennrich<sup>2</sup>, D. B. Kieda<sup>13</sup>, J. Kildea<sup>14</sup>, M. J. Lang<sup>9</sup>, Kuen Lee<sup>4</sup>, P. Moriarty<sup>15</sup>, J. Quinn<sup>7</sup>, M. Quinn<sup>15</sup>, B. Power-Mooney<sup>7</sup>, G. H. Sembroski<sup>9</sup>, S. P. Wakely<sup>16</sup>, V. V. Vassiliev<sup>8</sup>, T. C. Weekes<sup>1</sup>, J. Zweerink<sup>8</sup>

## ABSTRACT

The BL Lacertae (BL Lac) object 1ES 2344+514 (1ES 2344), at a redshift of 0.044, was discovered as a source of very high energy (VHE) gamma rays by the Whipple Collaboration in 1995 (Catanese et al. 1998). This detection was recently confirmed by the HEGRA Collaboration (Tluczykont et al. 2003). As

---

<sup>1</sup>Whipple Observatory, Harvard-Smithsonian Center for Astrophysics, P.O. Box 6369, Amado, AZ 85645-0097

<sup>2</sup>Dept. of Physics and Astronomy, Iowa State University, Ames, IA 50011-3160

<sup>3</sup>Department of Physics, Faculty of Science, Tanta University, Tanta 31527, Egypt

<sup>4</sup>Department of Physics, Washington University, St. Louis, MO 63130, USA

<sup>5</sup>Instituto de Fisica de Cantabria (CSIC-UC), Avenida de los Castros s/n, 39005 Santander, Spain

<sup>6</sup>Department of Physics, Grinnell College, Grinnell, IA 50112-1690, USA

<sup>7</sup>Experimental Physics Department, National University of Ireland, Belfield, Dublin 4, Ireland

<sup>8</sup>Department of Physics and Astronomy, University of California, Los Angeles, CA 90095-1547, USA

<sup>9</sup>Department of Physics, Purdue University, West Lafayette, IN 47907, USA

<sup>10</sup>Physics Department, National University of Ireland, Galway, Ireland

<sup>11</sup>School of Physics and Astronomy, University of Leeds, Leeds, LS2 9JT, UK

<sup>12</sup>Department of Physics and Astronomy, DePauw University, Greencastle, IN 46135-0037, USA

<sup>13</sup>Physics Department, University of Utah, Salt Lake City, UT 84112, USA

<sup>14</sup>Physics Department, McGill University, Montreal, QC H3A 2T8, Canada

<sup>15</sup>Department of Physical and Life Sciences, Galway-Mayo Institute of Technology, Dublin Road, Galway, Ireland

<sup>16</sup>Enrico Fermi Institute, University of Chicago, Chicago, IL 60637, USA

is typical for high-frequency peaked blazars, the VHE gamma-ray emission is highly variable. On the night of 20 December, 1995, a gamma-ray flare of 5.3-sigma significance was detected, the brightest outburst from this object to-date. The emission region is compatible with a point source. The spectrum between 0.8 TeV and 12.6 TeV can be described by a power law

$$\frac{d^3N}{dE dA dt} = (5.1 \pm 1.0_{st} \pm 1.2_{sy}) \times 10^{-7} (E/\text{TeV})^{-2.54 \pm 0.17_{st} \pm 0.07_{sy}} \frac{1}{\text{TeV m}^2 \text{ s}}.$$

Comparing the spectral index with that of the other five confirmed TeV blazars, the spectrum of 1ES 2344 is similar to 1ES 1959+650, located at almost the same distance. The spectrum of 1ES 2344 is steeper than the brightest flare spectra of Markarian 421 (Mrk 421) and Markarian 501 (Mrk 501), both located at a distance about 2/3 that of 1ES 2344, and harder than the spectra of PKS 2155-304 and H 1426+428, which are located almost three times as far. This trend is consistent with attenuation caused by the infrared extragalactic background radiation.

*Subject headings:* BL Lacertae objects: individual(1ES 2344+514)— gamma rays: observations

## 1. Introduction

To date, the only confirmed extragalactic gamma-ray sources at energies  $> 100$  GeV (very high energy, VHE) are BL Lacertae (BL Lac) objects and the giant radio galaxy M87 (Beilicke et al. 2004). BL Lac objects are active galactic nuclei (AGN) with (1) characteristic radio/optical/X-ray flux, (2) the absence of emission lines with observed equivalent width greater than  $5\text{\AA}$ , and (3) a CA II "break strength" smaller than 25% (Perlmutter et al. 1996). These criteria define an object with strong nonthermal emission which almost completely masks the thermal emission from the surrounding host galaxy. The spectrum, in a  $\nu F_\nu$  representation, shows a double-peaked structure. The only type of BL Lac objects detected so far to emit VHE emission are high-frequency peaked. For these objects, the low-energy component peaks in the soft to hard X-ray regime and the high-energy component peaks in the VHE regime. The six confirmed VHE BL Lac objects are: Mrk 421 (Punch et al. 1992; Petry et al. 1996), Mrk 501 (Quinn et al. 1996; Bradbury et al. 1997), 1ES 2344+514 (Catanese et al. 1998; Tluczykont et al. 2003), 1ES 1959+650 (Nishiyama et al. 1999; Holder et al. 2003; Aharonian et al. 2003), PKS 2155-304 (Chadwick et al. 1999; Aharonian et al. 2005), and H 1426+428 (Horan et al. 2002; Aharonian et al. 2002a). The emission level

around the two peaks is highly variable, and changes in the spectral shape with flux level have been measured for Mrk 421 (Krennrich et al. 2002; Aharonian et al. 2002b; Krennrich et al. 2003), Mrk 501 (Djannati-Atai et al. 1999; Aharonian et al. 2001), and 1ES 1959+650 (Aharonian et al. 2003). For the other three BL Lacs, variations of the spectral shape with flux level have neither been established nor ruled out.

The VHE observations reported here were carried out by the VERITAS (previously Whipple Gamma Ray) collaboration using an imaging atmospheric Cherenkov telescope (Weekes et al. 1989). The telescope, of 10 m diameter, is located on Mt. Hopkins at an altitude of 2320 m above sea level. At the time of observations, the imaging camera consisted of 109 photomultiplier tubes, each viewing  $0.259^\circ$  of the sky and arranged in a closed-packed hexagonal pattern. The telescope and the data acquisition are described in Cawley et al. (1990).

The organization of this paper is as follows: The status of observations on 1ES 2344 is summarized in Section 2. The VHE data and analysis techniques are presented in Section 3. This is followed in Section 4 by a description of the gamma-ray simulations necessary for the spectral reconstruction, including estimation of the gamma-ray energy in Sect. 4.1. The measured VHE spectra are presented in Section 5 and are briefly discussed and summarized in Section 6.

## 2. Observational Status of 1ES 2344+514

The BL Lac object, 1ES 2344+514, at a redshift of 0.044, was detected in the Einstein Slew Survey (Elvis et al. 1992) in the energy range 0.2-4 keV. The survey was constructed from data collected during the HEAO-2 mission from 1978-1981. 1ES 2344 was identified as a BL Lac object in Perlman et al. (1996). The non-contemporaneous spectral energy distribution of 1ES 2344 is shown in Figure 1. Observations at all wavelengths show 1ES 2344 to be an unresolved point source. The central black-hole mass is  $10^{8.80 \pm 0.16} M_\odot$ , derived from stellar velocity dispersion measurements (Barth et al. 2003). In the optical regime, a point source with an underlying elliptical host galaxy can be fitted with a radius (half-width at half-maximum) of  $r_e = 7.12 \pm 0.02$  kpc ( $H_0 = 50$  km s $^{-1}$  Mpc $^{-1}$  and  $q_0 = 0$ ) (Urry et al. 2000).

The optical and far-infrared emission from 1ES 2344 contains significant contributions from the host galaxy. The total photometry by the 2 Micron All Sky Survey (Jarrett et al. 2003) and by the Hubble Space Telescope (HST) (Urry et al. 2000), labeled "Galaxy light" in Figure 1, lie well above the value expected from pure synchrotron emission in the jet. Observations with the HST in 1996 measured a R-band brightness of the nucleus of  $16.83 \pm 0.05$

mag from a fit of a point source plus galaxy convolved with the point spread function of the telescope (Urry et al. 2000). During continued monitoring through 1998, the R-band brightness varied between 16.47 mag (Nilsson et al. 1999) and 17.00 mag (Falomo and Kotilainen 1999), indicating optical variability. An optical monitoring program in 2000/1 by Xie et al. (2002) found short time scale variability to be weak, with maximum intraday variability of  $\Delta V = 0.18$  mag,  $\Delta R = 0.1$  including galaxy light. A relatively large brightness decrease of 0.35 mag was observed in the V-band over 2 weeks in January 2001.

1ES 2344 showed X-ray variability on the time scale of a few hours in the 0.1 - 10 keV energy band during a week-long campaign in 1996 using the BeppoSAX satellite (Giommi et al. 2000). A follow-up observation in 1998 found 1ES 2344 to be in a very low state, implying a frequency shift by a factor of 30 or more of the peak synchrotron emission. They suggested the interpretation that two distinct electron populations contribute to the synchrotron emission; one steady low-energy component, the other producing soft to hard X-rays with rapid time variability.

1ES 2344 has been monitored by the Whipple Collaboration since 1995 (Catanese et al. 1998). Recently, the HEGRA Collaboration reported an independent confirmation of this source (Tluczykont et al. 2003). On the night of 5 December, 1996, Whipple VHE and BeppoSAX X-ray observations overlapped for 28 minutes, for which we show the X-ray spectrum and VHE flux upper limit in Figure 1. The 99.9% VHE flux upper limit at energies  $> 350$  GeV was calculated as in Catanese et al. (1998).

In the VHE band, the object was observed in a flaring state during the night of 20 December, 1995, with a significance of  $5.3 \sigma$ , the strongest gamma-ray flare measured from this object to date. The quiescent flux level of 1ES 2344, compared to the flare presented here, is about 50 times lower (Tluczykont et al. 2003). The detection of VHE gamma rays from 1ES 2344 in December 1995, reported by the Whipple Collaboration at the 1997 International Cosmic Ray Conference (Catanese et al. 1997), was considered tentative because follow-up observations by this and other VHE observatories through 1997 did not detect further evidence for gamma-ray emission. Monitoring by the Whipple Collaboration from 1998 to 2000, however, showed again a small positive excess (Badran 2001). A summary of all published VHE observations of this source is given in Table 1. An initial measurement of the VHE gamma-ray spectrum covering the entire 1995/6 observing season yielded a spectrum of  $(1.14 \pm 0.50) \times 10^{-7} E^{-2.29 \pm 0.43} \text{ TeV}^{-1} \text{ m}^{-2} \text{ s}^{-1}$ , statistical error only, over the energy range  $0.5 < E < 5.0$  TeV with  $\chi^2/ndf = 3.2/2$  (Bussons-Gordo 1998a,b).

In Figure 2, we show the two-dimensional gamma-ray sky map during the flare. The gamma-ray map was constructed from a partial data set, referred to as 'B' in Section 4. The emission region is compatible with a point source. This was determined using a Monte-

Carlo simulation of the telescope response to a point source of gamma rays. A small telescope pointing error of less than  $0.05^\circ$  may have been present during the observations, but due to the lack of bright stars in the field of view, we are not able to determine this in retrospect. The centroid of the measured gamma-ray emission is displaced from the known location of 1ES 2344 by RA  $0.02 \pm 0.02^\circ$  and DEC  $0.03 \pm 0.02^\circ$ . Within a conservatively estimated  $0.1^\circ$  circle of confusion are located three galaxies and two radio sources, but no other X-ray sources. Thus, the gamma-ray emission likely originated from 1ES 2344.

The EGRET 95% confidence level upper limit for 1ES 2344 is  $6.98 \times 10^{-8}$  cts  $\text{cm}^{-2} \text{s}^{-1}$ ,  $E > 100$  MeV (Hartman et al. 1999). The peak response for most sources detected with EGRET lies at around 300 MeV, this corresponds to an upper limit at 300 MeV of about  $3.4 \times 10^{-11} \text{erg cm}^{-2}$ .

### 3. Gamma-Ray Flare and Background Data

Observations with the 10 m telescope were carried out in two pointing modes: (1) with the source in the center of the field of view (ON observation) and (2) with the telescope pointing offset from the source direction by 30 minutes in RA, called OFF observation. The OFF observation is a measurement of the background caused by cosmic rays. On the night of 20 December, 1995, four ON observations were taken with a combined exposure time was 110 minutes. The last ON observation during the night was not complemented with an OFF observation, as is necessary for spectral measurements. Therefore, an OFF observation was selected from the 1995/6 season based on its similarity to the ON observation in elevation, cosmic-ray rate, and night sky brightness. For each ON observations, Table 2 lists the UTC start time, the average observing elevation, the throughput factor for both, ON and OFF observations, and the measured gamma-ray rate. The throughput factor measures the cosmic-ray rate relative to a reference observation taken under clear skies (Lebohec and Holder 2003). The weather during these observations was rated "A" by the observers, meaning clear skies. Figure 3 confirms this by comparing these observations with other "A" weather observations taken between October 1995 and April 1996.

The standard analysis method for data taken with the 10 m telescope (Reynolds et al. 1993) includes conditioning of the images, parameterization, and selection of gamma-ray like events. Conditioning of the images consists of: (1) flat-fielding of the relative gain between pixels, (2) equalizing the sky brightness between the ON and OFF observation (Cawley 1993), and (3) removing pixels that are below a certain signal-to-noise ratio. Images are then parameterized by their RMS *width* and *length*, their *distance* from the center of the field of view (Hillas 1985), and the orientation angle of their major axis relative to the

pointing direction of the telescope, *alpha* (Weekes et al. 1987). The total amount of light collected is referred to as the *size* of the image.

The gamma-ray signal is derived from the excess number of events between ON and OFF runs, where only those images are selected that are likely to have been produced by a gamma-ray source located at the center of the field of view. The rate given in Table 2 shows the gamma-ray rate after application of one particular set of selection criteria (cuts), called *Supercuts*1995 (Catanese et al. 1998). These cuts are not optimal for spectral measurements because the selection efficiency for gamma-rays decreases dramatically with energy. Therefore, a different set of cuts was developed empirically using simulated gamma-ray events, see Section 4.1. The analysis of the data given in Table 2 is in agreement with a previous analysis by Catanese et al. (1998).

#### 4. Calibration and Spectral Reconstruction

The data contain a relatively low gamma-ray rate and were taken over a wide range of elevations. To obtain an accurate energy calibration our analysis technique requires us to analyze different elevation ranges separately. To maintain a good signal-to-noise ratio, the data were combined at the two average elevations of  $58^\circ$  and  $41^\circ$  and referred to as datasets A and B, respectively. The data in these two sets were taken sequentially during the night, allowing us to investigate time variability in the emission level.

A total of 500,000 gamma-ray initiated showers were simulated at each elevation; these were distributed in energy randomly according to a power law of index -2.5 and covering a circular area around the telescope axis. The Monte-Carlo simulations of gamma-ray initiated particle showers in the atmosphere and subsequent detection of Cherenkov photons by the telescope were carried out with the Grinnell-ISU (GrISU) package<sup>1</sup>. At  $58^\circ$  elevation, simulations were carried out over the energy range 0.1-100 TeV and impact radius less than 300 m. At  $41^\circ$  elevation, simulations were carried out over the energy range 0.3-100 TeV and impact radius less than 350 m. The low-energy cut-off was chosen to extend beyond the range of energies of events that trigger the telescope. The night-sky brightness level of simulated showers was matched to that measured from the data.

The absolute light throughput of the telescope was calibrated with Cherenkov images of muons recorded by the telescope. For this, only complete muon rings were selected using a specially developed algorithm (Schroedter 2004). This ensures that the total amount of

---

<sup>1</sup>Available at <http://www.physics.utah.edu/gammaray/GrISU/>

light is well known. The light throughput factor derived in this way was used to measure the spectrum of the Crab Nebula during 1995/6 season. With statistical (st) and systematic (sy) errors, the spectrum of the Crab Nebula between 0.3 TeV and 13 TeV can be fitted by  $(4.2 \pm 0.3_{st} \pm 0.7_{sy}) \times 10^{-7} E^{-2.38 \pm 0.08_{st} \pm 0.04_{sy}} \text{ TeV}^{-1} \text{ m}^{-2}\text{s}^{-1}$  with  $\chi^2_{min}/\text{ndf} = 3.2/(9-2)$ . This is compatible with other measurements (Mohanty et al. 1998; Hillas et al. 1998).

The energy resolution of the spectral analysis depends on rejecting cosmic-ray images, and selecting only those gamma-ray images with well defined image parameters. The collection area near the triggering threshold is difficult to model in the simulations and hence a software cut on the minimum brightness is applied that lies substantially above the hardware threshold. The following set of loose cuts were then applied to data and simulations:  $0.31^\circ < \text{distance} < 1.1^\circ$ ,  $\text{length}/\text{size} < 0.00085^\circ/\text{dc}$ ,  $\text{max2} > 65 \text{ dc}$ , and  $\text{alpha} < 25^\circ$ .

The differential trigger rates at  $41^\circ$  elevation, data set B, are shown in Figure 4 for a spectrum with differential index of -2.5. The peak trigger rate occurs at an energy of 1.4 TeV for spectral cuts, described below, and 2.1 TeV with *Supercuts*1995. With these cuts, 90% of the triggers occur above 1.05 TeV and 1.67 TeV, respectively. The collection area, shown in Figure 5, reaches 10% of its maximum value of  $170,000 \text{ m}^2$  at an energy of about 1.1 TeV for spectral cuts. The differential trigger rates at  $58^\circ$  elevation, corresponding to data set A, are shown in Figure 4. The peak trigger rate occurs at an energy of 0.69 TeV for spectral cuts and 1.1 TeV with *Supercuts*1995. For these two sets of cuts, 90% of the triggers occur above 0.48 TeV and 0.75 TeV, respectively. The collection area, shown in Figure 5, reaches 10% of its maximum value of  $136,000 \text{ m}^2$  at an energy of about 0.51 TeV for spectral cuts.

#### 4.1. Event Selection and Energy Estimation

The spectral analysis method has been described in Petry et al. (2002); Mohanty et al. (1998). Simulations at  $41^\circ$  elevation show an energy resolution of  $\text{rms}(\Delta \log E) = 0.15$  or  $\text{rms}(\Delta E/E) = 0.40$ , with an energy estimation bias of  $|\Delta \log E| = 0.018$  over the energy region  $E = 0.8 \text{ TeV}$  to  $40 \text{ TeV}$ . This energy range begins at 10% of the peak collection area. A cut-off at the high energies is necessary as the limited field of view of the camera truncates large showers and the estimated and true energies begin to diverge. At  $58^\circ$  elevation, the energy resolution is  $\text{rms}(\Delta \log E) = 0.16$  or  $\text{rms}(\Delta E/E) = 0.49$  and  $|\Delta \log E| = 0.012$  over the energy range  $E = 0.4 \text{ TeV}$  to  $25 \text{ TeV}$ .

The gamma-ray signal is contaminated by a large fraction of cosmic-ray events. To reject this background, cuts are imposed on the parameters *distance*, *width*, *length*, and *alpha*. The cuts derived from the Monte-Carlo simulations scale with *size* so that the efficiency of

selecting gamma rays remains unchanged as a function of energy. The fraction of gamma rays passing the cuts for simulations at  $41^\circ$  elevation is 86%, and it is 87% at  $58^\circ$  elevation. The distributions of the parameters *width*, *length*, and *alpha* are shown for simulated gamma rays in Figure 6. The cuts are chosen at a nominal 2 standard deviations around the mean value. The simulations at  $58^\circ$  are limited by statistics at high energies, making the cuts somewhat inefficient. In particular, the upturn at large dc value of the *alpha*-cut is unphysical, but the cut-level still remains below the *Supercuts1995* value of  $15^\circ$ . The unphysical upturn is due to the second order polynomial used in fitting the cut-level. For comparison, the level of *Supercuts1995* is also shown in Figure 6.

## 5. Flare Spectra

The number of excess gamma-ray events in each energy bin after application of all cuts is presented for both data sets in Tables 3 and 4. Due to the very small signal, the bin width is chosen at twice the energy resolution  $\Delta(\log E) = 0.3$  (Petry et al. 2002). Flux upper limits are given if the gamma-ray significance is less than  $1\sigma$  in the energy bin. The upper limits are at the 98% confidence level and calculated according to the method of Helene (1983). The spectra for the two data sets A and B are shown in Figure 7. The error bars show the statistical error only.

For dataset B, the power law fit to the spectrum over the energy range from 0.8 TeV to 12.6 TeV is given by

$$\frac{dN}{dE dA dt} = (5.1 \pm 1.0_{st} \pm 1.2_{sy}) \times 10^{-7} E^{-2.54 \pm 0.17_{st} \pm 0.07_{sy}} \frac{1}{\text{TeV m}^2 \text{ s}}, \quad (1)$$

with  $\chi^2_{min}/ndf = .2/(4 - 2)$ . The  $\chi^2$  probability for this data to randomly arise from the power-law fit is 0.9. The statistical error represents the 68% confidence interval (CI) for a fit with one free parameter while the other parameter is frozen at its optimum value. The 68% CI with two simultaneous free parameters, defined by  $\chi^2_{min} + 2.3$ , is shown in Figure 8.

The systematic errors of the flux constant and spectral index arising from the energy calibration and the cut-tolerance are indicated in Figure 8 by crosses. The cut tolerance, with a nominal value of 2 standard deviations, was varied between 1.5 and 2.5 standard deviations; the level of the muon-based energy calibration is  $\pm 10\%$ . The uncertainty in the energy calibration affects mostly the flux constant. For example, a 10% change in the energy calibration changes the flux constant by 25% (30%) if the spectrum has a differential index of -2.5 (-3.0). In addition, due to the large elevation range covered, a small systematic uncertainty on the order of 10-15% is intrinsic to the GrISU simulations (Krennrich et al. 1999). The spectral index is affected mostly by varying the cut tolerance. It should be



noted that the systematic error evaluated in this way is smaller than the statistical error. This means that a good estimate of the systematic error is not possible with this method; nevertheless it does indicate the relative importance of the two sources of error.

For data set A, the power law fit over the energy range from 0.4 TeV to 1.6 TeV is given by

$$\frac{dN}{dE dA dt} = (1.9 \pm 0.6_{st} \pm 0.6_{sy}) \times 10^{-7} E^{-3.3 \pm 0.7_{st} \pm 0.7_{sy}} \frac{1}{\text{TeV m}^2 \text{ s}}, \quad (2)$$

and the confidence interval contours are shown in Figure 8.

As the spectral indexes of the two spectra are compatible, it is possible to adjust the flux constant of the less significant spectrum (set A) so that it overlaps, in a least-squares sense, with the spectrum of set B. However, as the statistical significance of data set A is very small compared to set B, combining the two data sets results in an insignificant improvement in the statistical error of the spectral index. Therefore, the spectral measurement of 1ES 2344 derived here, is best represented by spectrum of data set B, alone.

## 6. Discussion

1ES 2344 is a variable source; during the flare on 20 December, 1995, the gamma-ray emission from 1ES 2344 was about 50 times brighter than during the quiescent phase measured several years later. To obtain an accurate energy calibration, our analysis technique required us to analyze data taken at different observing elevations separately. Therefore, we split the data into two sets, A and B, with 56 and 38 minutes exposure time, respectively. The data sets were taken consecutively during the night. The spectral indices measured from the two data sets are compatible with each other. The increase of the flux constant over the two hours of observation, though also not very significant, is not unexpected as very large variability of the VHE flux on time scale of hours has been observed for other blazars (Gaidos et al. 1996; Quinn et al. 1996; Holder et al. 2003; Aharonian et al. 2005).

The measured VHE spectra are attenuated through pair production with the infrared extragalactic background light (EBL) (Nikishov 1962). Due to the EBL spectral shape, the attenuation manifests itself as a steepening of the measured VHE spectrum between roughly 1 and 5 TeV and becomes more pronounced with larger redshift. A cut-off feature is thus expected in the VHE spectra, if variations in the intrinsic VHE spectrum are ignored. Such a cut-off feature has been established for Mrk 421 and Mrk 501 (Aharonian et al. 2001; Krennrich et al. 2001, 2002). Their spectra can be described with a power law with exponential cut-off:  $dN/dE \propto E^{-\alpha} \exp(E/E_0)$ . The cut-off energy,  $E_0$ , differs between the two blazars by  $2.6 \pm 1.2$  TeV (Aharonian et al. 2002b). Unfortunately, for 1ES 2344 the low

statistical significance of the spectrum precludes the measurement of such a cut-off energy.

VHE spectra are now available for all six confirmed TeV blazars. The power law spectral indexes of fits to the brightest flares from the blazars appear to steepen with redshift (Schroedter 2005). The spectral index of the 1ES 2344 VHE flare is steeper than the brightest flare spectra of Mrk 421 and Mrk 501, both located at about 2/3 the distance of 1ES 2344. The flare spectra of PKS 2155-304 and H 1426+428, located almost three times as far, are softer than that of 1ES 2344. The spectral index of the 1ES 2344 flare is similar to the flare spectrum of 1ES 1959+650, which is located at almost the same redshift. This trend is consistent with attenuation caused by the infrared extragalactic background radiation (Schroedter 2005; Stecker 1999). Alternatively, galaxy evolution might be responsible for the observed spectral steepening with redshift. For example, if younger galaxies have enhanced mid-infrared radiation nearer to the central black hole, then this would produce gamma-ray attenuation indistinguishable from that caused by the EBL.

No contemporaneous measurements at other wavelengths were taken during the gamma-ray flare of 1ES 2344 on 20 December, 1995. This precludes the application of models to constrain the gamma-ray production mechanism, because the gamma-ray emission is known to be highly variable. Almost one year later, on 5 December, 1996, a simultaneous TeV / X-ray observation occurred together with the *BeppoSAX* satellite. The detailed X-ray spectrum measured during this night (Giommi et al. 2000) is complemented, however, only by an upper limit of the TeV flux, again precluding models to be significantly constrained.

We acknowledge the technical assistance of K. Harris, T. Lappin, and E. Roache. This research has made use of the NASA/IPAC Extragalactic Database (NED) which is operated by the Jet Propulsion Laboratory, California Institute of Technology, under contract with the National Aeronautics and Space Administration.

## REFERENCES

- Aharonian F, Akhperjanian A, Barrio J, et al. TeV gamma rays from the blazar H 1426+428 and the diffuse extragalactic background radiation. *A&A*, 384:L23–L26, Mar. 2002a.
- Aharonian F, Akhperjanian A, Barrio J, et al. The TEV Energy Spectrum of Markarian 501 Measured with the Stereoscopic Telescope System of HEGRA during 1998 and 1999. *ApJ*, 546:898–902, Jan. 2001.

- Aharonian F, Akhperjanian A, Beilicke M, et al. Variations of the TeV energy spectrum at different flux levels of Mkn 421 observed with the HEGRA system of Cherenkov telescopes. *A&A*, 393:89–99, Oct. 2002b.
- Aharonian F, Akhperjanian A, Beilicke M, et al. Detection of TeV gamma-rays from the BL Lac 1ES 1959+650 in its low states and during a major outburst in 2002. *A&A*, 406: L9–L13, July 2003.
- Aharonian F, Akhperjanian AG, Aye KM, et al. H.E.S.S. observations of PKS 2155-304. *A&A*, 430:865–875, Feb. 2005.
- Aharonian FA, Akhperjanian AG, Barrio JA, et al. HEGRA search for TeV emission from BL Lacertae objects. *A&A*, 353:847–852, Jan. 2000.
- Badran HM. Recent Observations of 1ES 2344+514 Using the Whipple Gamma-Ray Telescope. In *AIP Conf. Proc. 587: Gamma 2001: Gamma-Ray Astrophysics*, pages 281–285, 2001.
- Barth AJ, Ho LC, Sargent WLW. The Black Hole Masses and Host Galaxies of BL Lacertae Objects. *ApJ*, 583:134–144, Jan. 2003.
- Beilicke M et al. Observations of the giant radio galaxy M87 at TeV energies with H.E.S.S. In *XXII Texas Symposium on Relativistic Astrophysics*, 2004. astro-ph/0504395.
- Bradbury SM, Deckers T, Petry D, et al. Detection of  $\gamma$ -rays above 1.5TeV from MKN 501. *A&A*, 320:L5–L8, Apr. 1997.
- Bussons-Gordo J. *Derivation of the TeV Gamma-Ray Spectrum of Three Active Galaxies: Mrk 421, Mrk 501, and 1ES 2344+514*. PhD thesis, University College Dublin, July 1998a.
- Bussons-Gordo J. The TeV Energy Spectrum of the Active Galaxies 1ES 2344+514 and Markarian 501. In *Proceedings 16th ECRS, July 20-24*, pages 379+, 1998b.
- Catanese M, Akerlof CW, Badran HM, et al. Discovery of Gamma-Ray Emission above 350 GeV from the BL Lacertae Object 1ES 2344+514. *ApJ*, 501:616–623, July 1998.
- Catanese M, Boyle PJ, Burdett AM, et al. First Results from a Search for TeV Emission from BL Lacs Out to  $Z = 0.2$ . In *Proceedings of the 25th ICRC*, volume 3, pages 277–280, 1997.
- Cawley MF. The Application of Noise Padding to the Cherenkov Imaging Technique. In *Towards a Major Cerenkov Detector*, pages 176–181. Universal Academy Press, 1993.

- Cawley MF, Fegan DJ, Harris K, et al. A high resolution imaging detector for TeV gamma-ray astronomy. *Experimental Astronomy*, 1:173–193, 1990.
- Chadwick PM, Lyons K, McComb TJL, et al. Very High Energy Gamma Rays from PKS 2155-304. *ApJ*, 513:161–167, Mar. 1999.
- Djannati-Atai A, Piron F, Barrau A, et al. Very High Energy Gamma-ray spectral properties of MKN 501 from CAT Čerenkov telescope observations in 1997. *A&A*, 350:17–24, Oct. 1999.
- Douglas JN, Bash FN, Bozayan FA, et al. The Texas Survey of Radio Sources Covering  $-35.5$  degrees  $<$  declination  $<$  71.5 degrees at 365 MHz. *AJ*, 111:1945–1963, May 1996.
- Elvis M, Plummer D, Schachter J, et al. The Einstein Slew Survey. *ApJS*, 80:257–303, May 1992.
- Falomo R, Kotilainen JK. Optical imaging of the host galaxies of X-ray selected BL Lacertae objects. *A&A*, 352:85–102, Dec. 1999.
- Gaidos JA, Akerlof CW, Biller SD, et al. Extremely rapid bursts of TeV Photons from the active galaxy Markarian 421. *Nature*, 383:319–320, 1996.
- Giommi P, Padovani P, Perlman E. Detection of exceptional X-ray spectral variability in the TeV BL Lac 1ES 2344+514. *MNRAS*, 317:743–749, Oct. 2000.
- Gregory PC, Condon JJ. The 87GB catalog of radio sources covering delta between O and  $+ 75$  deg at 4.85 GHz. *ApJS*, 75:1011–1291, Apr. 1991.
- Hartman RC, Bertsch DL, Bloom SD, et al. The Third EGRET Catalog of High-Energy Gamma-Ray Sources. *ApJS*, 123:79–202, July 1999.
- Helene O. Upper limit of peak area. *Nuclear Instruments and Methods in Physics Research A*, 212:319–322, Dec. 1983.
- Hillas AM. Čerenkov light images of EAS produced by primary gamma. *NASA. Goddard Space Flight Center 19th Intern. Cosmic Ray Conf., Vol. 3 p 445-448 (SEE N85-34862 23-93)*, 3:445–448, Aug. 1985.
- Hillas AM, Akerlof CW, Biller SD, et al. The Spectrum of TeV Gamma Rays from the Crab Nebula. *ApJ*, 503:744–759, Aug. 1998.
- Holder J, Bond IH, Boyle PJ, et al. Detection of TeV Gamma Rays from the BL Lacertae Object 1ES 1959+650 with the Whipple 10 Meter Telescope. *ApJ*, 583:L9–L12, Jan. 2003.

- Horan D, Badran HM, Bond IH, et al. Detection of the BL Lacertae Object H1426+428 at TeV Gamma-Ray Energies. *ApJ*, 571:753–762, June 2002.
- Jarrett TH, Chester T, Cutri R, et al. The 2MASS Large Galaxy Atlas. *AJ*, 125:525–554, Feb. 2003.
- Konopelko A, Kettler J, HEGRA. TeV Gamma-Ray Observations of the BL Lac Object 1ES 2344+514 with the HEGRA System of Imaging Atmospheric Cherenkov Telescopes. In *Proceedings of the 26th ICRC*, volume 3, pages 426–429, 1999.
- Krennrich F, Badran HM, Bond IH, et al. Cutoff in the TeV Energy Spectrum of Markarian 421 during Strong Flares in 2001. *ApJ*, 560:L45–L48, Oct. 2001.
- Krennrich F, Biller SD, Bond IH, et al. Measurement of the Multi-TeV Gamma-Ray Flare Spectra of Markarian 421 and Markarian 501. *ApJ*, 511:149–156, Jan. 1999.
- Krennrich F, Bond IH, Bradbury SM, et al. Discovery of Spectral Variability of Markarian 421 at TeV Energies. *ApJ*, 575:L9–L13, Aug. 2002.
- Krennrich F et al. Hourly Spectral Variability of Mrk 421. In *Proceedings of the 28th ICRC*, 2003. URL astro-ph/0305419.
- Lebohec S, Holder J. The cosmic ray background as a tool for relative calibration of atmospheric Cherenkov telescopes. *Astroparticle Physics*, 19:221–233, May 2003.
- Mohanty G, Biller S, Carter-Lewis DA, et al. Measurement of TeV gamma-ray spectra with the Cherenkov imaging technique. *Astroparticle Physics*, 9:15–43, June 1998.
- Nikishov AI. Absorption of High-Energy Photons in the Universe. *Soviet Physics JETP*, 14: 393–394, Feb. 1962.
- Nilsson K, Pursimo T, Takalo LO, et al. Two-dimensional Photometric Decomposition of the TeV BL Lacertae Objects Markarian 421, Markarian 501, and 1ES 2344+514. *PASP*, 111:1223–1232, Oct. 1999.
- Nishiyama T et al. 1ES1959+650. In *Proceedings of the 26th ICRC*, volume 3, pages 370–373, 1999.
- Patnaik AR, Browne IWA, Wilkinson PN, et al. Interferometer phase calibration sources. I - The region 35–75 deg. *MNRAS*, 254:655–676, Feb. 1992.
- Perlman ES, Stocke JT, Schachter JF, et al. The Einstein Slew Survey Sample of BL Lacertae Objects. *ApJS*, 104:251–285, June 1996.

- Petry D, Bond IH, Bradbury SM, et al. The TeV Spectrum of H1426+428. *ApJ*, 580:104–109, Nov. 2002.
- Petry D, Bradbury SM, Konopelko A, et al. Detection of VHE  $\gamma$ -rays from MKN 421 with the HEGRA Cherenkov Telescopes. *A&A*, 311:L13–L16, July 1996.
- Punch M, Akerlof CW, Cawley MF, et al. Detection of TeV photons from the active galaxy Markarian 421. *Nature*, 358:477–478, Aug. 1992.
- Quinn J, Akerlof CW, Biller S, et al. Detection of Gamma Rays with E greater than 300 GeV from Markarian 501. *ApJ*, 456:L83–L86, Jan. 1996.
- Reynolds PT, Akerlof CW, Cawley MF, et al. Survey of candidate gamma-ray sources at TeV energies using a high-resolution Cerenkov imaging system - 1988-1991. *ApJ*, 404: 206–218, Feb. 1993.
- Schroedter M. *The Very High Energy Gamma-Ray Spectra of AGN*. PhD thesis, University of Arizona, 2004.
- Schroedter M. Upper Limits on the Extragalactic Background Light from the Very High Energy Gamma-Ray Spectra of Blazars. *ApJ*, 2005.
- Stecker FW. Intergalactic extinction of high energy gamma-rays. *Astroparticle Physics*, 11: 83–91, June 1999.
- Stevens JA, Gear WK. Variations in the broad-band spectra of BL Lac objects: millimetre observations of an X-ray-selected sample. *MNRAS*, 307:403–412, Aug. 1999.
- Thuczykont M, Götting N, Heinzelmann G, et al. Observations of 54 Active Galactic Nuclei with the HEGRA Cherenkov Telescopes. In *Proceedings of the 28th ICRC*, volume 5, pages 2547–2550, 2003.
- Urry CM, Scarpa R, O’Dowd M, et al. The Hubble Space Telescope Survey of BL Lacertae Objects. II. Host Galaxies. *ApJ*, 532:816–829, Apr. 2000.
- Weekes TC, Cawley MF, Fegan DJ, et al. Observation of TeV gamma rays from the Crab nebula using the atmospheric Cerenkov imaging technique. *ApJ*, 342:379–395, July 1989.
- Weekes TC, Lamb RC, Hillas AM. HERCULES - A new instrument for TeV astronomy. In *NATO ASIC Proc. 199: Very High Energy Gamma Ray Astronomy*, pages 235–242, 1987.

White RL, Becker RH. A new catalog of 30,239 1.4 GHz sources. *ApJS*, 79:331–467, Apr. 1992.

Xie GZ, Zhou SB, Dai BZ, et al. Photometric monitoring of 12 BL Lacertae objects. *MNRAS*, 329:689–699, Feb. 2002.

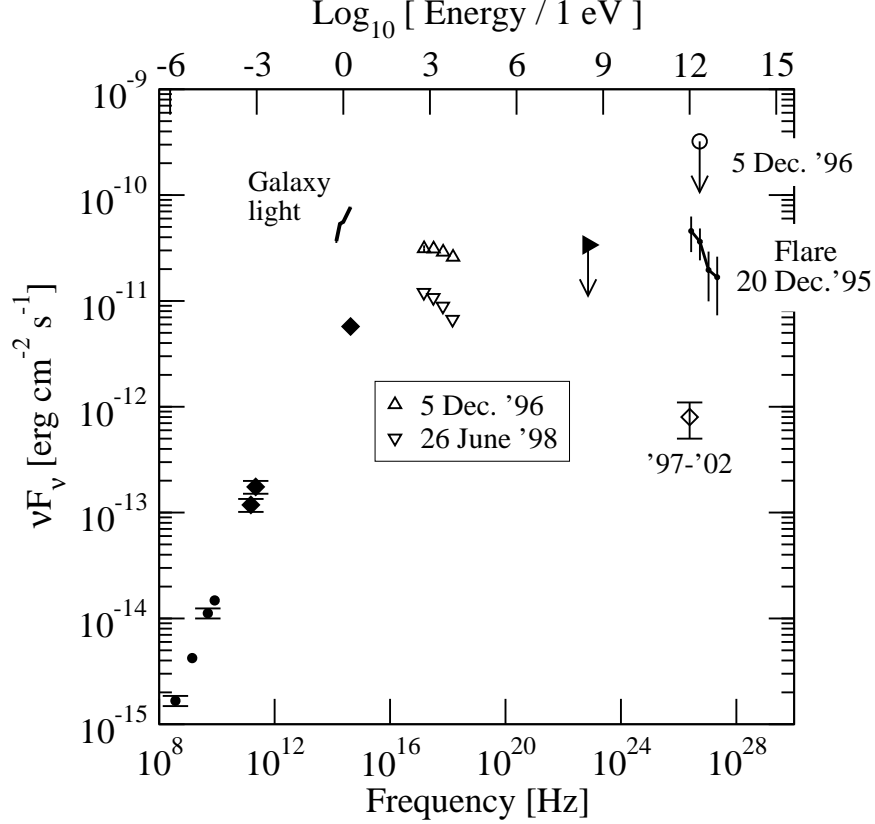


Fig. 1.— The spectral energy distribution of 1ES 2344 along with the VHE flare spectrum obtained with the Whipple 10 m telescope (*line with error bars*). Also shown is the VHE flux upper limit for the night of 5 December, 1996 (*open circle*). Other data were taken from the following sources: 365 MHz from Texas radio survey (*filled circle*) (Douglas et al. 1996), 1.4 GHz from Greenbank (*filled circle*) (White and Becker 1992), 4.85 GHz from Greenbank (*filled circle*) (Gregory and Condon 1991), 8.4 GHz from VLA (*filled circle*) (Patnaik et al. 1992), galaxy photometry at millimeter wavelength (*filled diamond*) (Stevens and Gear 1999), galaxy photometry at K, H, and J-bands from 2MASS (*line segment*) (Jarrett et al. 2003), galaxy and nucleus R-band photometry obtained with Hubble Space Telescope and corrected for interstellar reddening (*filled diamond*) (Urry et al. 2000). X-ray observation with BeppoSAX (*see legend*) from (Giommi et al. 2000), upper limit at 300 MeV from EGRET (*filled triangle*) (Hartman et al. 1999). Quiescent VHE gamma ray flux during the period 1997-2002 from HEGRA (*open diamond*) (Tluczykont et al. 2003).



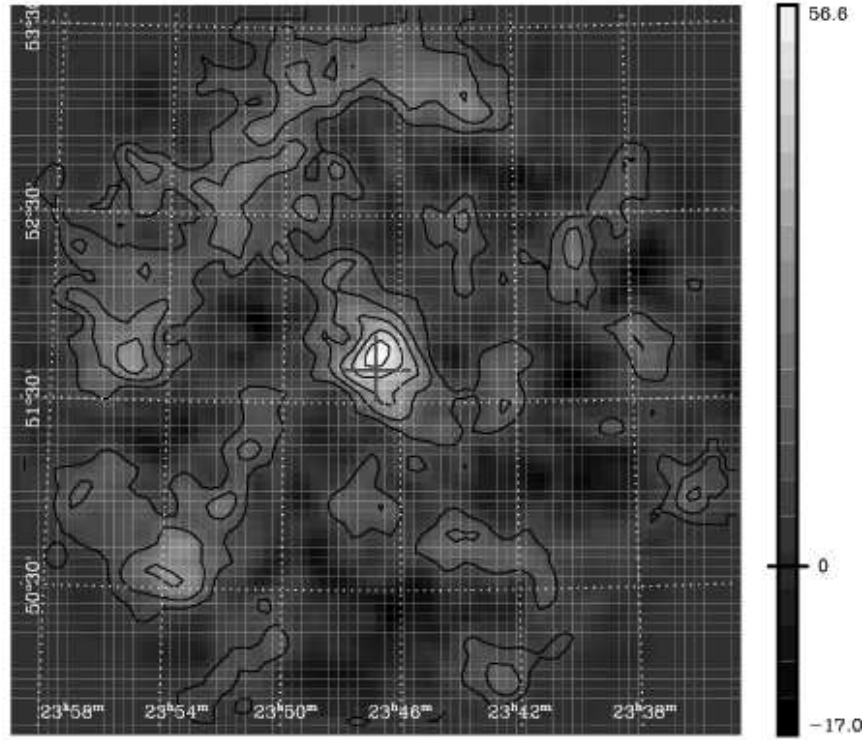


Fig. 2.— Gamma-ray sky map of the field of view around 1ES 2344, with position indicated by the *red cross*. The colors show excess counts with overlaid significance contours in steps of one standard deviation per contour. The *dotted* lines show the RA and DEC.

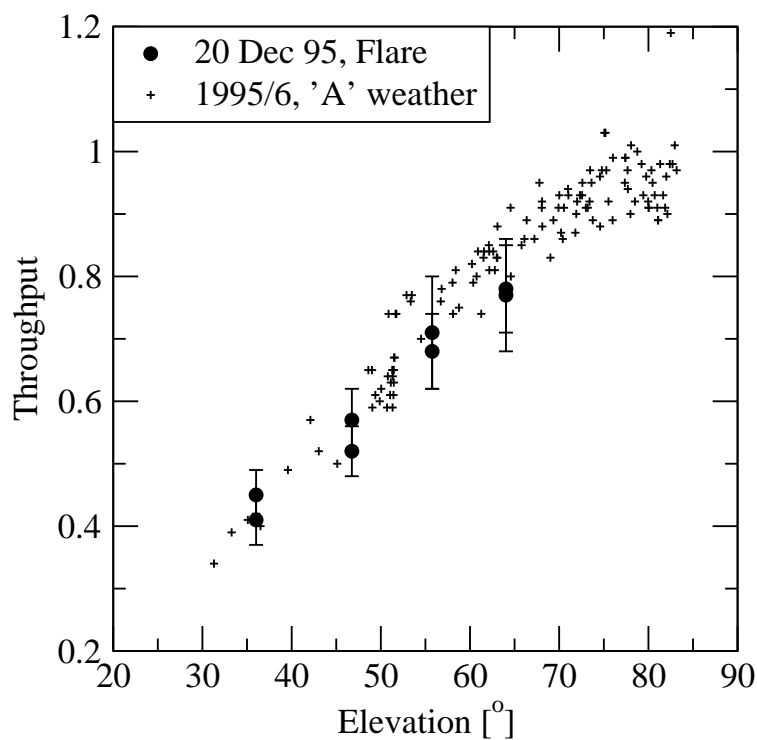


Fig. 3.— Relative cosmic ray rate of 1ES 2344 flare data compared to observations carried out under clear skies (rated “A” by observers) in 1995/6. For clarity, the error bars are only shown for the flare data.

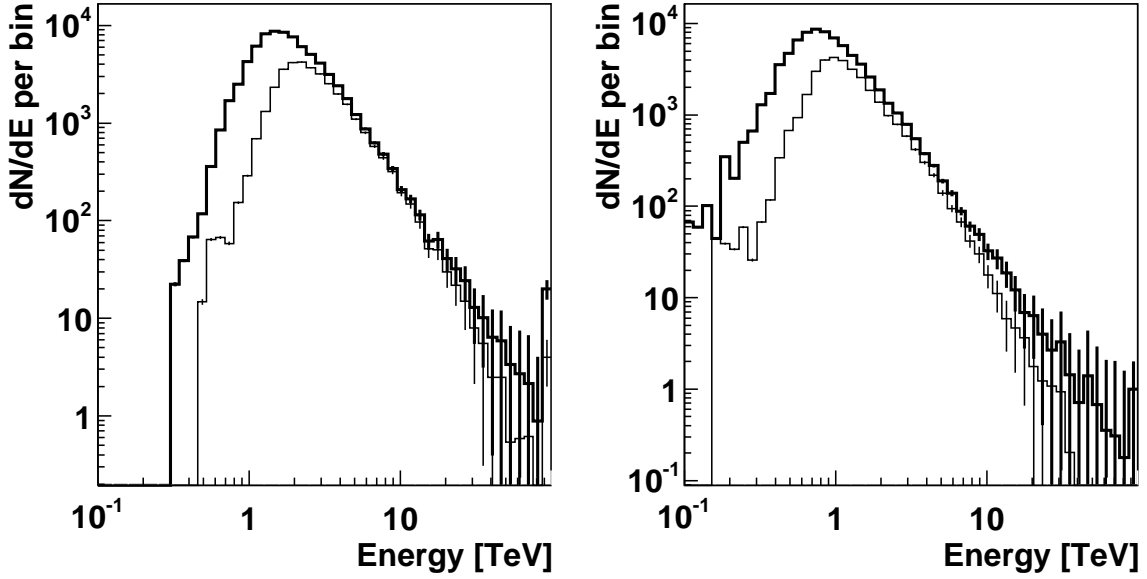


Fig. 4.— Simulated trigger rate at 41° elevation (*left*) and 58° (*right*) of gamma-rays distributed with a power law index of -2.5. The two lines show the rate after application of spectral cuts (*bold*) and *Supercuts1995* (*thin*).

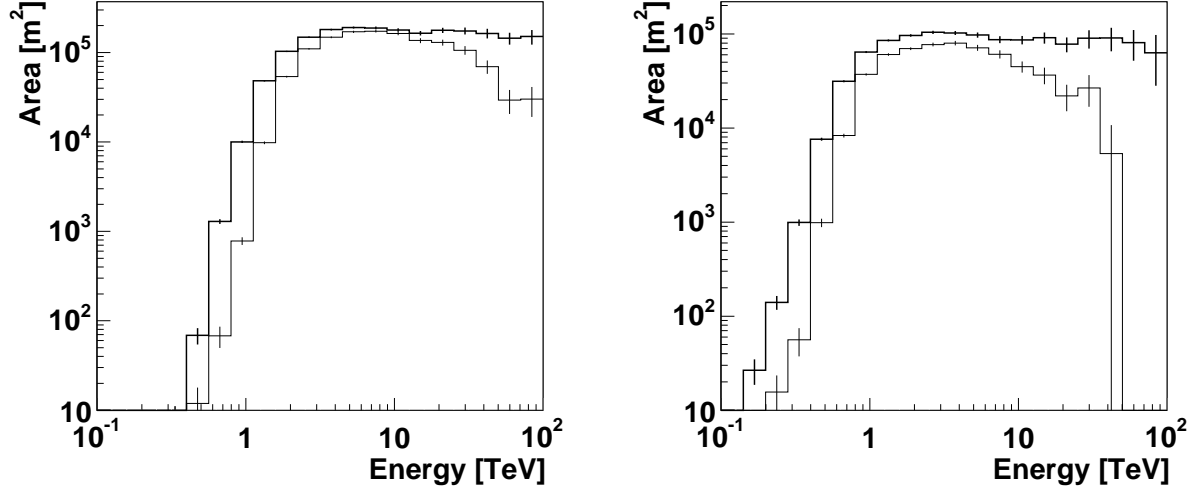


Fig. 5.— Collection area for gamma rays at 41° elevation (*left*) and at 58° elevation (*right*) in 1995 for spectral cuts (bold line) and *Supercuts1995* cuts (thin line).

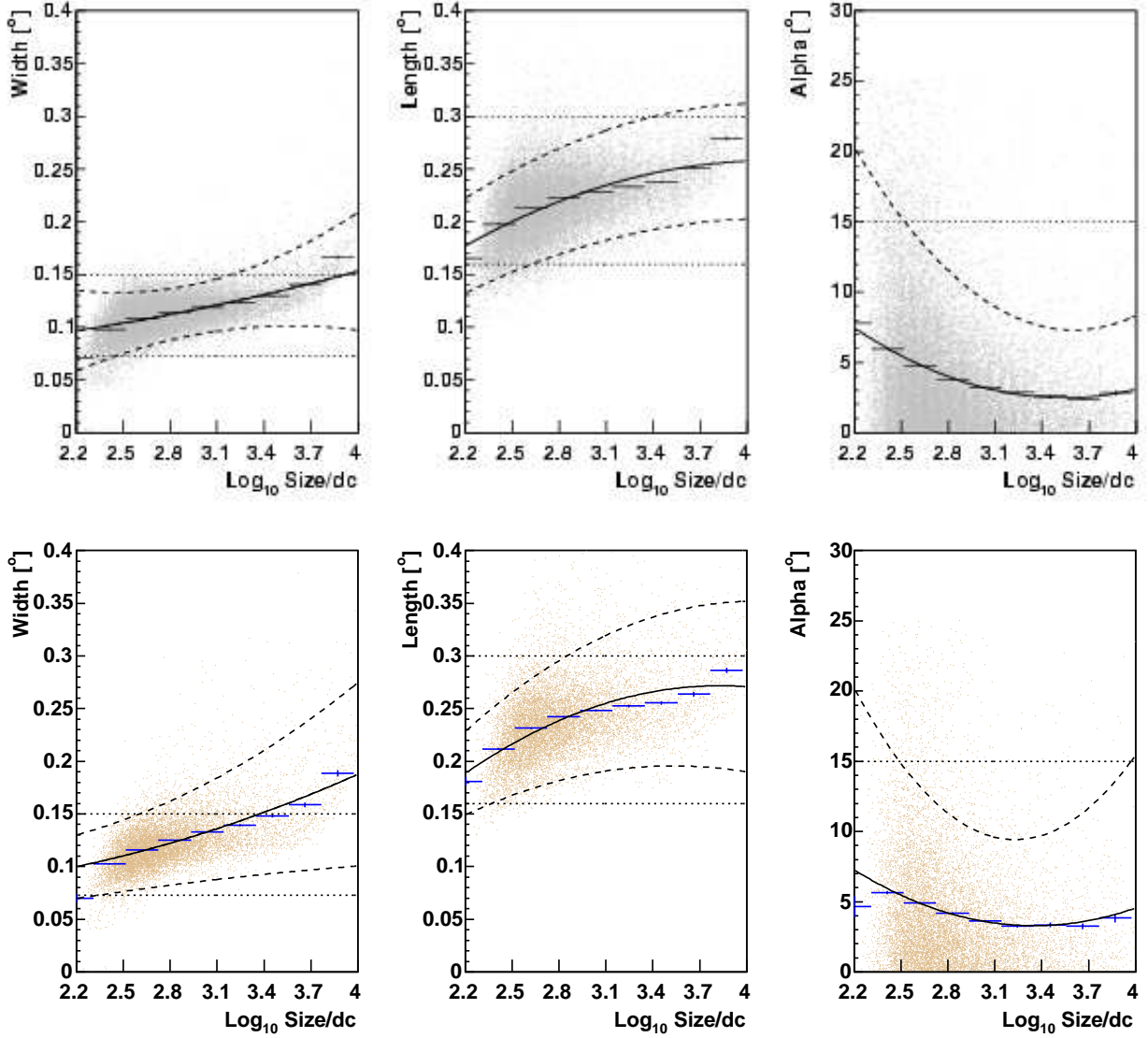


Fig. 6.— Simulated parameter distributions and cut levels with  $\log(\text{size})$  after application of loose cuts, see text. *Top row*: simulated at  $41^\circ$  elevation, *bottom row*:  $58^\circ$  elevation. The *dots* are simulated events and *crosses* represent the average. The *solid lines* shows the fitted polynomial to the average. *Dashed lines* show the actual cut chosen at a tolerance of two standard deviations around the average. *Dotted lines* show the cut level of *Supercuts1995*.

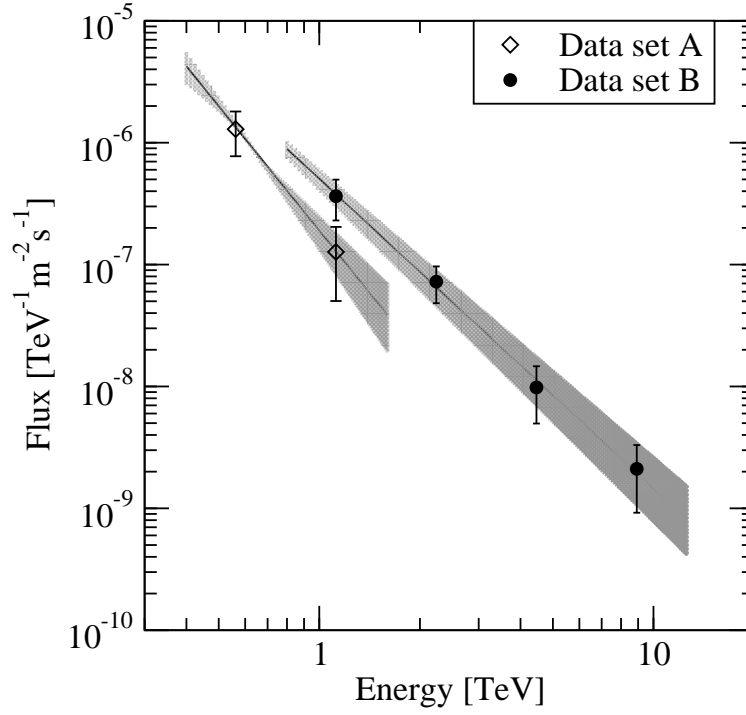


Fig. 7.— Differential flux spectrum of 1ES 2344 on 20 December 1995. Spectra from data sets A (*diamonds*) and B (*circles*) are shown together with power law fits (*solid lines*). The shaded regions show the confidence interval of the power law fits and were obtained by varying both parameters to their individual 68% confidence interval.

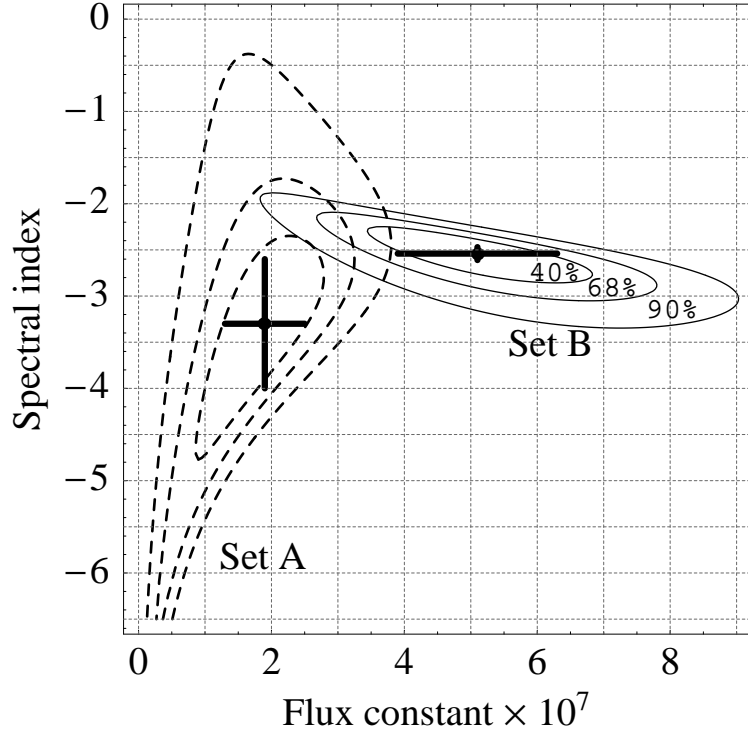


Fig. 8.— Confidence regions corresponding to spectrum of data set A (*dashed lines*) and set B (*solid lines*). Confidence regions are shown with probability content of 40%, 68%, and 90% for the simultaneous values of the spectral index and flux constant. Also shown are the systematic error on the flux constant and spectral index (*crosses*)

Table 1: Summary of VHE measurements of 1ES 2344.

Date	Reference	Exposure [hr]	S <sup>a</sup> [ $\sigma$ ]	Integral Flux [ $\times 10^{-7} \text{ m}^{-2} \text{s}^{-1}$ ]	$E_{thresh}$ [TeV]
1995/6	Catanese et al. 1998	20.5	5.8	$1.7 \pm 0.5$	0.35
20 Dec. 1995	Catanese et al. 1998	1.85	5.3 <sup>b</sup>	$6.6 \pm 1.9$	0.35
1996/7	Catanese et al. 1998	24.9	0.4	$< 0.82^c$	0.35
Dec. 1997	Aharonian et al. 2000	15.8	NA	$< 0.29^d$	1.0
1997-2002	Tluczykont et al. 2003	72.5	4.4	$0.08 \pm 0.03$	0.8
1998	Konopelko et al. 1999	23.8	3.3 <sup>b</sup>	$< 0.09^d$	1.0
2000	Badran 2001	3.1	2.4	$1.1 \pm 0.1^e$	$\approx 0.4$

---

<sup>a</sup>Statistical excess.

<sup>b</sup>Part of the data listed in the above entry.

<sup>c</sup>99.9% C.L. upper limit

<sup>d</sup>99% C.L. upper limit

<sup>e</sup>Statistical error only.



Table 2: Details of the observations taken on 20 Dec. 1995.

UTC <sup>a</sup>	El.	Throughput <sup>b</sup>	$\gamma$ -rate <sup>c</sup>
2:32	64°	0.77/0.78 $\pm$ 0.08	0.70 $\pm$ 0.28
3:34	55°	0.68/0.71 $\pm$ 0.08	1.04 $\pm$ 0.37
4:35	47°	0.52/0.57 $\pm$ 0.05	0.91 $\pm$ 0.42
5:36	37°/36°	0.45/0.41 $\pm$ 0.04	1.54 $\pm$ 0.47
Average			1.14 $\pm$ 0.20

---

<sup>a</sup>Start time of the ON observation. The first three ON observations lasted for 28 minutes followed by an OFF observation. The last observation had a length of only 10 min. A complementary OFF observation, necessary for the spectral analysis, was chosen based upon similar observation conditions.

<sup>b</sup>Relative cosmic-ray rate for ON/OFF observation, see text.

<sup>c</sup>Gamma-ray rate per minute after *Supercuts*1995 (Catanese et al. 1998).

Table 3: Event statistics and flux in each energy bin for data set A. Upper limits are given at the 98% confidence level.

Energy [TeV]	ON [events]	OFF [events]	ON-OFF [events]	S [ $\sigma$ ]	Flux [TeV <sup>-1</sup> m <sup>-2</sup> s <sup>-1</sup> ]
0.56	63	38	25 $\pm$ 10	2.5	(1.29 $\pm$ 0.51) $\times 10^{-6}$
1.12	83	63	20 $\pm$ 12	1.7	(1.27 $\pm$ 0.77) $\times 10^{-7}$
2.24	39	42	-3 $\pm$ 9	-0.3	<3.91 $\times 10^{-8}$
4.47	22	19	3 $\pm$ 6	0.5	<1.46 $\times 10^{-8}$
8.91	8	7	1 $\pm$ 4	0.3	<3.62 $\times 10^{-9}$
Total	220	174	44 $\pm$ 19.8	2.2	

Table 4: Event statistics and flux in each energy bin for data set B. Upper limits are given at the 98% confidence level.

Energy [TeV]	ON [events]	OFF [events]	ON-OFF [events]	S [ $\sigma$ ]	Flux [TeV <sup>-1</sup> m <sup>-2</sup> s <sup>-1</sup> ]
1.12	55	30	25 $\pm$ 9	2.7	(3.64 $\pm$ 1.34) $\times 10^{-7}$
2.24	86	51	35 $\pm$ 12	3.0	(7.24 $\pm$ 2.42) $\times 10^{-8}$
4.47	35	20	15 $\pm$ 7	2.0	(9.82 $\pm$ 4.85) $\times 10^{-9}$
8.91	14	6	8 $\pm$ 4	1.8	(2.11 $\pm$ 1.19) $\times 10^{-9}$
17.78	7	4	3 $\pm$ 3	0.9	<1.19 $\times 10^{-9}$
35.48	0	2	-2 $\pm$ 1	-1.4	<1.43 $\times 10^{-10}$
Total	197	113	84 $\pm$ 17.6	4.8	